Journal of Nanobiotechnology

RESEARCH

Open Access

Platelet-rich plasma-derived exosomes promote blood-spinal cord barrier repair and attenuate neuroinflammation after spinal cord injury

Xinyu Nie[1†], Yanting Liu[2†], Tianyang Yuan[1], Tong Yu[1], Zhihe Yun[1], Wu Xue[1], Tao Yu[1], Junyan An[1], Anyuan Dai[1], Kun Wu[1] and Qinyi Liu[1*]

Abstract

Spinal cord injury (SCI) compromises the blood-spinal cord barrier (BSCB) and induces neuroinflammation, potentially exacerbating neuronal damage. This underscores the importance of maintaining BSCB integrity and mitigating neuroinflammation in SCI treatment. Our study explores an innovative approach to treating SCI by utilizing platelet-rich plasma-derived exosomes (PRP-Exos) to stabilize BSCB function and alleviate neuroinflammation. We successfully isolated exosomes from platelet-rich plasma and conducted both in vivo and in vitro experiments to assess the therapeutic effects of PRP-Exos and explore their potential mechanisms in stabilizing the BSCB, reducing neuroinflammation, and promoting neural functional recovery.In vitro results demonstrate that PRP-Exos significantly reduce the permeability of bEnd.3 cells under hypoxic-hypoglycemic conditions, thereby restoring the integrity of tight junctions. Additionally, our study elucidates the critical role of the NF-κB signaling pathway in the amelioration of neuroinflammation by PRP-Exos. In the SCI model, local injection of hydrogel-encapsulated PRP-Exos reduced Evans blue dye leakage, enhanced the expression of tight junction proteins, alleviated the inflammatory environment in the damaged area, and improved neural functional recovery. In conclusion, PRP-Exos presents a promising and effective treatment option for SCI.

Keywords Platelet-rich plasma(PRP), Spinal cord injury, Exosomes, Blood-spinal cord barrier, Neuroinflammation

[†]Xinyu Nie and Yanting Liu contributed equally to this work.

*Correspondence:
Qinyi Liu
qinyi@jlu.edu.cn
[1]Department of Orthopaedic, The second hospital of Jilin University, Changchun, China
[2]Department of Neurosurgery, Seoul St. Mary's Hospital, College of Medicine, The Catholic University of Korea, Seoul, South Korea

Introduction

Spinal cord injury (SCI) represents a prevalent form of central nervous system trauma, leading to the loss of motor and sensory functions and adversely impacting the physical and social well-being of affected individuals [1]. Traumatic SCI triggers hypoxia at the lesion site, leading to the disruption of the blood-spinal cord barrier (BSCB), and the infiltration of pro-inflammatory cytokines, neutrophils, and macrophages, resulting in secondary damage. This secondary damage initiates neuronal and glial cell death, inflammatory responses, and the formation of glial fibrotic scars, ultimately hindering axonal regeneration [2, 3].Therefore, in therapeutic strategies for SCI, maintaining the integrity of the BSCB and mitigating neuroinflammation are crucial for promoting the recovery of neural functions following spinal cord damage.

Currently, most treatments for SCI are palliative and unable to halt disease progression or replace apoptotic neurons [4, 5]. There is an urgent need for effective treatments that can promote the recovery of spinal cord functions and improve the quality of life for patients. Platelet-rich plasma (PRP) is an autologous blood product containing a high concentration of platelets and various growth factors. The growth factors and cytokines released by platelets play a key role in tissue regeneration and repair, hence PRP has increasingly gained clinical attention [6–8].

However, the clinical application of PRP is limited due to its dependency on autologous platelets [9]. Beyond growth factors, platelet activation also leads to the secretion of extracellular vesicles, including exosomes (Exos, 30–200 nm in diameter). Exosomes, discovered over recent decades, can serve as carriers for bioactive proteins, mRNA, and microRNA, facilitating intercellular communicatio [10–12]. Exosomes derived from diverse sources, notably mesenchymal stem cells, are currently employed in spinal cord injury repair research. These exosomes function both as therapeutic agents and delivery vehicles, playing integral roles in the regeneration process [13–15].PRP-derived exosomes (PRP-Exos) have shown great potential in tissue repair and regeneration, possessing anti-inflammatory properties and positively regulating cellular bioactivity [16–20]. PRP-Exos can transport key factors such as transforming growth factor beta 1 (TGF-β1), platelet-derived growth factor-BB (PDGF-BB), vascular endothelial growth factor (VEGF), and stromal cell-derived factor 1 (SDF-1), thereby enhancing their therapeutic effects. Furthermore, PRP-Exos exhibit low immunogenicity and stability, making them ideal carriers for clinical nanotherapies [21]. However, their application in central nervous system disorders has not been reported.

In this study, we utilized a double centrifugation method to extract PRP and subsequently isolated and characterized PRP-Exos. Our investigation centered on the role of PRP-Exos in stabilizing the BSCB, mitigating neuroinflammation, and facilitating the recovery of neurological function. In our in vivo experiments, we utilized hydrogel as a delivery medium for PRP-Exos to achieve these objectives. Moreover, we delved into the molecular mechanisms underlying the neuroinflammatory alleviation by PRP-Exos, particularly highlighting the critical involvement of the NF-κB signaling pathway in this process. Overall, our findings suggest that PRP-Exos effectively stabilizes the BSCB, reduces neuroinflammation, and enhance functional recovery post-SCI, thereby underscoring their potential as a promising therapeutic approach for SCI treatment.

Materials and methods

PRP extraction and activation

Whole blood samples were collected from healthy rats and mixed with acid-citrate dextrose solution A (ACD-A) in anticoagulant tubes (1 ml ACD-A per 9 ml blood, Sigma, USA) following the protocols of Tao et al. and Guo et al. [18, 19]. After centrifugation at 160 g for 10 min, the platelet-containing plasma was carefully aspirated and transferred to a new centrifuge tube and then centrifuged again at 250 g for 15 min. The supernatant plasma was discarded, and the platelet pellet was resuspended in the residual plasma to obtain 4 ml of PRP.PRP samples were then subjected to centrifugation at 250 g for 15 min to pellet the platelets, which were subsequently washed with Phosphate buffered saline (PBS)(Gibco, USA). Activation of PRP was achieved by incubating with 10% $CaCl_2$ and 1000 U thrombin [22] (Beyotime, Beijing, China), for 30 s, followed by centrifugation at 300 g for 10 min and 2000 g for 10 min to remove cellular debris.

Isolation and characterization of PRP-Exos

PRP was purified using the exoEasy Maxi Kit (Qiagen, Germany) as previously described, following the manufacturer's protocols. The isolated exosomes (PRP-Exos) were stored at −80 °C freezer for further use. Transmission electron microscopy (TEM; Hitachi, Japan) was employed to visualize the morphology of PRP-Exos, while Nanosight tracking analysis (NTA; PARTICLE METRIX- ZetaVIEW, Germany) was utilized to determine their concentration and size distribution. Additionally, the presence of exosomal markers CD9 and CD81 was confirmed by western blot.

Cell culture

The BV-2 and b.End 3 cell lines were obtained from Cyagen (China) and cultured in DMEM medium (Gibco, USA) supplemented with 100 U/mL penicillin, 100 μg/mL streptomycin (Gibco, USA), and 10% fetal bovine serum (HKA, China).

Uptake of Exos by bEnd.3 and BV-2

To label PRP-Exos for tracking purposes, DiL (1,1'-dioctadecyl-3,3,3',3'-tetramethylindocarbocyanine perchlorate) solution (Umibio, China) was added to PBS and incubated following the manufacturer's instructions. After centrifugation at 100,000 g at 4 °C for 1 h to remove excess dye, the DiL-labeled PRP-Exos (80 μg/1 ml) were co-cultured with bEnd.3 and BV-2 cells for 6 h. Subsequently, cells were washed three times with PBS, fixed in 4% paraformaldehyde (PFA), permeabilized with 0.05% Triton X-100 for 5 min, and incubated with FITC-Phalloidin (Beyotime, Beijing, China). Nuclei were counterstained with DAPI dihydrochloride, and fluorescent images were acquired using a confocal laser scanning microscope (Olympus, Japan).

Oxygen glucose deprivation and reoxygenation (OGD/R)

To simulate the in vivo ischemic-hypoxic environment, bEnd.3 cells were subjected to OGD/R as previously described [23]. Upon reaching full confluence, the culture medium was replaced with glucose-free DMEM (Gibco, USA), and the cells were incubated in an Anaero-Pack (oxygen concentration < 0.2%) (Mitsubishi, Japan) at 37 °C for 6 h. Subsequently, the cells were transferred to normal growth conditions for reoxygenation experiments for 24 h (DMEM with 10% FBS under normoxia).

Trans-endothelial permeability assay in vitro

Trans-endothelial permeability was assessed using FITC-dextran (40 kDa, 1 mg/mL; Sigma, USA). bEnd.3 cells were seeded in the upper insert and allowed to reach full confluence. The upper insert was filled with 100 μL of FITC-dextran, while the lower chamber contained 500 μL of medium. After 1 h of incubation in sheltered light, fluorescence measurements were performed using a fluorescence spectrophotometer (BMG Labtech, USA).

Cell immunofluorescence staining

Immunofluorescence staining was conducted to assess the nuclear translocation of NF-κB p65 in Lipopolysaccharide (LPS)-exposed BV-2 cells and the integrity of the BSCB in vitro. Cells were fixed with paraformaldehyde for 15 min, permeabilized with 0.1% Triton-X100 for 5 min, and blocked with donkey serum for 4 h. Slides were then incubated with primary antibodies against NF-κB p65 (1:100, Proteintech, China), ZO-1 (1:100, Proteintech, China), and Claudin-3 (1:100, Proteintech, China), followed by treatment with a fluorochrome-conjugated donkey anti-rabbit secondary antibody (1:1000). After labeling the nuclei with DAPI, images were captured using a fluorescence microscope.

Real-time quantitative PCR

Cells were prepared using the RNA extraction kit (Takara Biotechnology, Japan). Following the measurement of RNA concentrations, 3 μg of RNA was reverse transcribed into cDNA using the PrimerScript® First Strand cDNA Synthesis Kit (Sigma-Aldrich, USA). The expression levels of M1 markers (IL-6, TNF-α, COX-2, and iNOS) and M2 markers (CD206, Ym-1, and Arg-1) were assessed with the SYBR Green Kit from South San Francisco, USA, and compared to β-actin expression using the 2-ΔΔCt technique. The primer sequences listed in Supplementary-Table 1.

Western blot

We extracted total proteins from cells and tissues using a protein extraction kit (Beyotime, Beijing, China) and quantified them to 40 g per 15 μL via using SDS and P0013B lysate. Protein samples were subjected to4%-12% SDS-PAGE and transferred onto PVDF membranes (Millipore, Billerica, MA, USA). 5% skim milk was used to block membranes, and primary antibodies were incubated overnight with phospho-NF-κB p65 (1:1000, Proteintech, China), NF-κB p65 (1:2000, Proteintech, China), phospho-iκb (1:2000, Proteintech, China), iκb (1:1000, Proteintech, China), and β-actin (1:3000, ServiceBio, China) .The membranes were washed with TBST three times per 10 min, incubated with secondary antibodies, and detected with ECL Luminous liquid.

ELISA

The cells were cultured in the 24-well plates. After incubation with PRP-Exos for 6 h and being stimulated with LPS (1 mg/mL) for 24 h, the protein expression of TNF-α and IL-6 in the supernatant was examined with the ELISA kits Systems, BioLegend, USA).

Preparation and characterization of the PRP-Exos/injectable hydrogel (PEG/ODEX hydrogel)

To ensure stable release of PRP-Exos in vitro, a previously reported hydrogel preparation method was employed [24]. Solutions of 4-arm-PEG-NH2 (12 mg/mL) and oxidized dextran (o-Dex) (8 mg/mL) were each dissolved in phosphate-buffered saline (PBS, pH 7.4). These solutions were then mixed in equal volumes and homogenized. Injectable hydrogels were formed by incubating the mixed solutions at 37 °C (Figure S1-A). To create PRP-Exos/Gel, PRP-Exos (160 μg/mL) were combined with the hydrogel in equal volumes to ensure homogeneous distribution of PRP-Exos within the gel matrix for controlled delivery.

PEG/ODEX hydrogel release profile of PRP-Exo/Gel

For release studies, the same amount of PRP-Exo/Gel was placed into 12 wells plate and incubated in medium at

37 °C. The supernatant was removed and fresh medium was added at different timepoints. The number of Exo released into the medium was determined using the Bicinchoninic Acid Assay (Thermo Scientific, USA).

SCI model and treatment

All procedures were performed in strict adherence to institutional animal welfare guidelines and received approval from the Animal Care and Use Committee at Jilin University. Following a 7-day acclimation, mice were randomly allocated into four experimental groups: Sham, SCI, Gel, and PRP-Exos/Gel. To establish the SCI model, mice were anesthetized with intraperitoneal injections of 0.3% pentobarbital sodium at a dosage of 60 mg/kg. Subsequently, the animals were immobilized in a prone position on a cork board, and a vertical incision of 1 cm was made from T8 to T10 along the spine to reveal the underlying vertebral columns. The T9 vertebra was located, and its bone was carefully excised to access the spinal cord beneath. A precise, moderate injury was then inflicted by clamping the spinal cord with a vascular clip for a duration of 30 s [25]. Treatment involved the application of 10 µL hydrogels directly at the lesion site through a microsyringe. The SCI group was administered 10 µL of sterile saline instead. Control animals were subjected to the same surgical procedures excluding the spinal injury. Postoperative care included measures for infection prevention, analgesia, hydration, and nutritional support. Housing was individual for each mouse, with manual assistance for urination provided thrice daily until they regained the ability to urinate autonomously.

Behavioral and weight assessments

Hindlimb motor function recovery post-SCI was monitored using the Basso Mouse Scale (BMS), assessing changes at predetermined time points (1, 7, 14, 21, and 28 days post-injury). This scale ranges from 0, indicating complete paralysis, to 9, representing normal motor function. Two independent evaluators, blind to the experimental conditions, conducted the assessments. The average of their scores was computed to establish the final BMS rating for each mouse. Digital photographs of the mice's hindlimb postures were taken on the 28th day. Concurrently, mice weights were recorded and compared at specific intervals (1, 7, 14, 21, 28 days).

Hematoxylin and eosin (H&E) and masson staining

Histological analyses were conducted on 5 µm sections of paraffin-embedded tissues, stained with hematoxylin and eosin (H&E) using established protocols. Imaging was performed with a VS200 digital slide scanner (Olympus, Japan), facilitating detailed tissue examination.

Determination of exosomes uptake in vivo

To track PRP-Exos in vivo, fluorescent-labeled exosomes were locally administered after the injury. 14 days after the injury, spinal cord tissue was collected and sectioned for immunostaining to analyze the uptake of exosomes by endothelial cells and microglia.

Immunofluorescence analysis

Spinal cord specimens were preserved in 4% paraformaldehyde (PFA, Solarbio), processed through a sucrose gradient, embedded in OCT (Sakura), and sectioned at 10 µm with a cryostat. For cellular assays, after 4% PFA fixation, cells underwent permeabilization (1% Triton X-100), blocking (5% normal goat serum), and overnight incubation with primary antibodies at 4 °C. Following incubation with fluorochrome-tagged secondary antibodies and PBS washes, nuclei were counterstained with DAPI. A VS200 digital slide scanner (Olympus, Japan) was employed for imaging.

Statistical analysis

Data were presented as mean ± SEM and analyzed using SPSS 13.0 software. Differences were evaluated using one-way analysis of variance (ANOVA) while multiple comparisons were performed with the least significant difference(LSD) method. A p-value < 0.05 was considered statistically significant, while a p-value < 0.01 was considered highly significant.

Results

Characterization of PRP exosomes

The purified PRP-Exos were characterized using a suite of techniques, including Transmission Electron Microscopy (TEM), Nanoparticle Tracking Analysis (NTA), and Western blotting. TEM analysis showed that the PRP-Exos are spherical nanoparticles with diameters ranging from 100 to 200 nm, consistent with sizes reported in existing studies (Fig. 1B). NTA results supported this finding, showing a similar distribution of particle sizes (refer to Fig. 1C), indicative of exosome presence. The identification of exosomal surface markers CD9 and CD81 through Western blotting further confirmed the exosomal nature of PRP-Exos (Fig. 1D). Additionally, confocal microscopy illustrated that PRP-Exos, when co-cultured with BV-2 cells for 6 h, progressively accumulated within the bEnd.3 and BV-2 cells, suggesting a time-dependent uptake by the bEnd.3 and BV-2 cells (refer to Fig. 1E and S1C).

PRP-Exos attenuate neuroinflammation in LPS-stimulated BV-2 cells

This section explores the impact of PRP-Exos on neuroinflammation, particularly focusing on their anti-inflammatory properties in BV-2 microglial cells. Initially, we

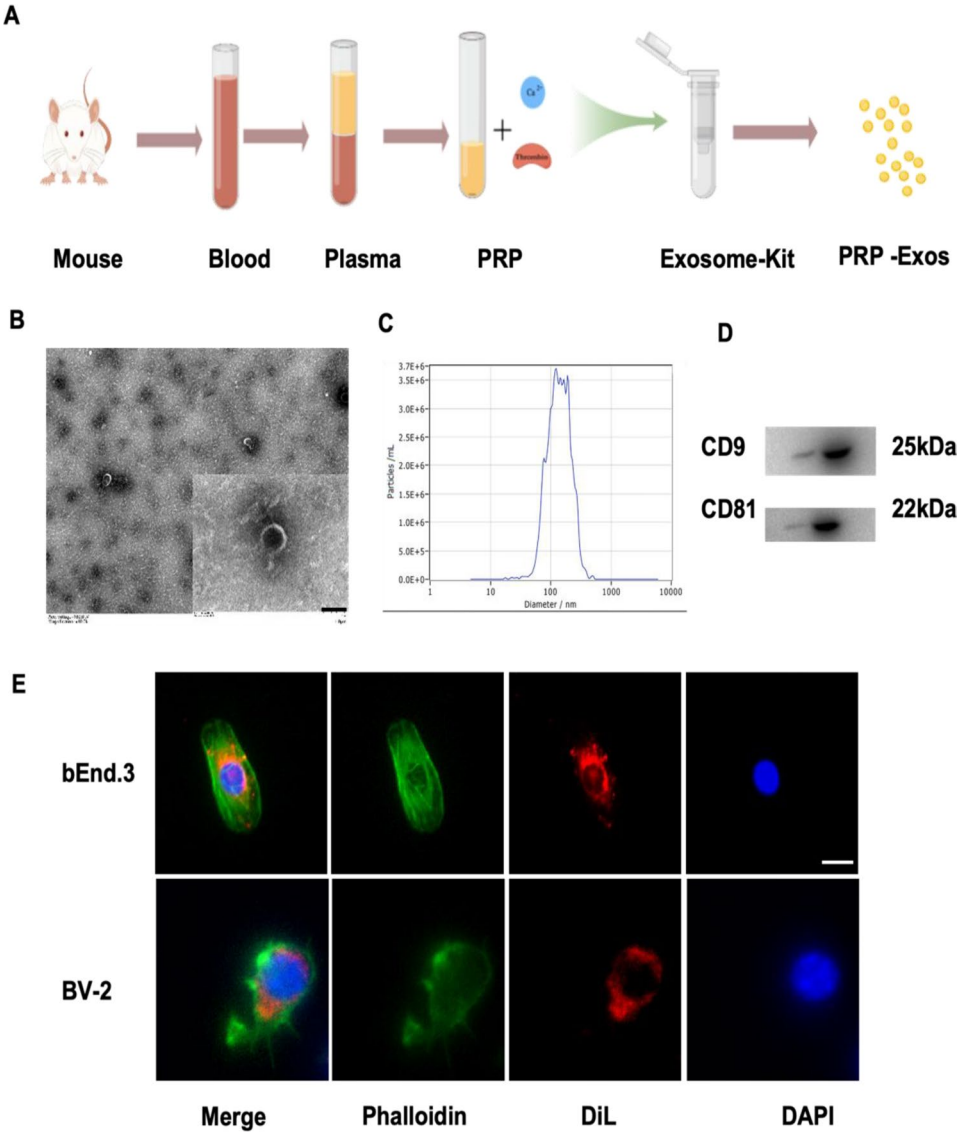

Fig. 1 Isolation and characterization of PRP-Exos. (**A**) Procedure for PRP-Exos Isolation; (**B**) Morphology of PRP-Exo examined by TEM. Scale bar: 100 μm; (**C**) Particle size distribution of Exo measured by NTA; (**D**) Western blotting analysis of the surface biomarkers CD9, and CD81 on PRP-Exo; (**E**) Fluorescent images of bEnd.3 and BV-2 cocultured with PRP-Exo showing that Exos could be taken up by bEnd.3 and BV-2. Scale bar: 10 μm

assessed the cytotoxic effects of PRP-Exos on BV-2 cells. Following this, we investigated the impact of PRP-Exos on the expression of microglial M1 and M2 phenotype markers. Cells were pre-treated with PRP-Exos for 6 h before being stimulated with LPS for 12 h (for mRNA levels) and 24 h (for protein levels). The expression levels of M1 and M2 phenotype markers were then quantified using RT-PCR, ELISA, and Western blot analyses. The findings revealed that PRP-Exos treatment led to a suppression of M1 phenotype markers, including IL-6 (Fig. 2A, G), TNF-α (Fig. 2B, H), iNOS (Fig. 2C, I, J), and COX-2 (Fig. 2D, I, L). Conversely, there was an upregulation of M2 markers, including Arg-1 (Fig. 2E, I, K), and Ym-1 (Fig. 2F, I, M). These data suggest that PRP-Exos can effectively reduce inflammatory responses in BV-2 cells exposed to LPS.

PRP-Exos inhibit NF-κB pathway activationy in LPS-stimulated BV-2 cells

The NF-κB pathway, critical in the inflammatory response, regulates the production of multiple pro-inflammatory mediators. This study aimed to uncover how PRP-Exos affect M1 and M2 microglia polarization by assessing their impact on the NF-κB signaling pathway. BV-2 cells, pre-treated with PRP-Exos for six hours, were subsequently exposed to LPS for one hour. We analyzed the phosphorylation of IκB and NF-κB p65 and the degradation of IκB through Western blotting. Moreover, the nuclear translocation of NF-κB p65 was evaluated

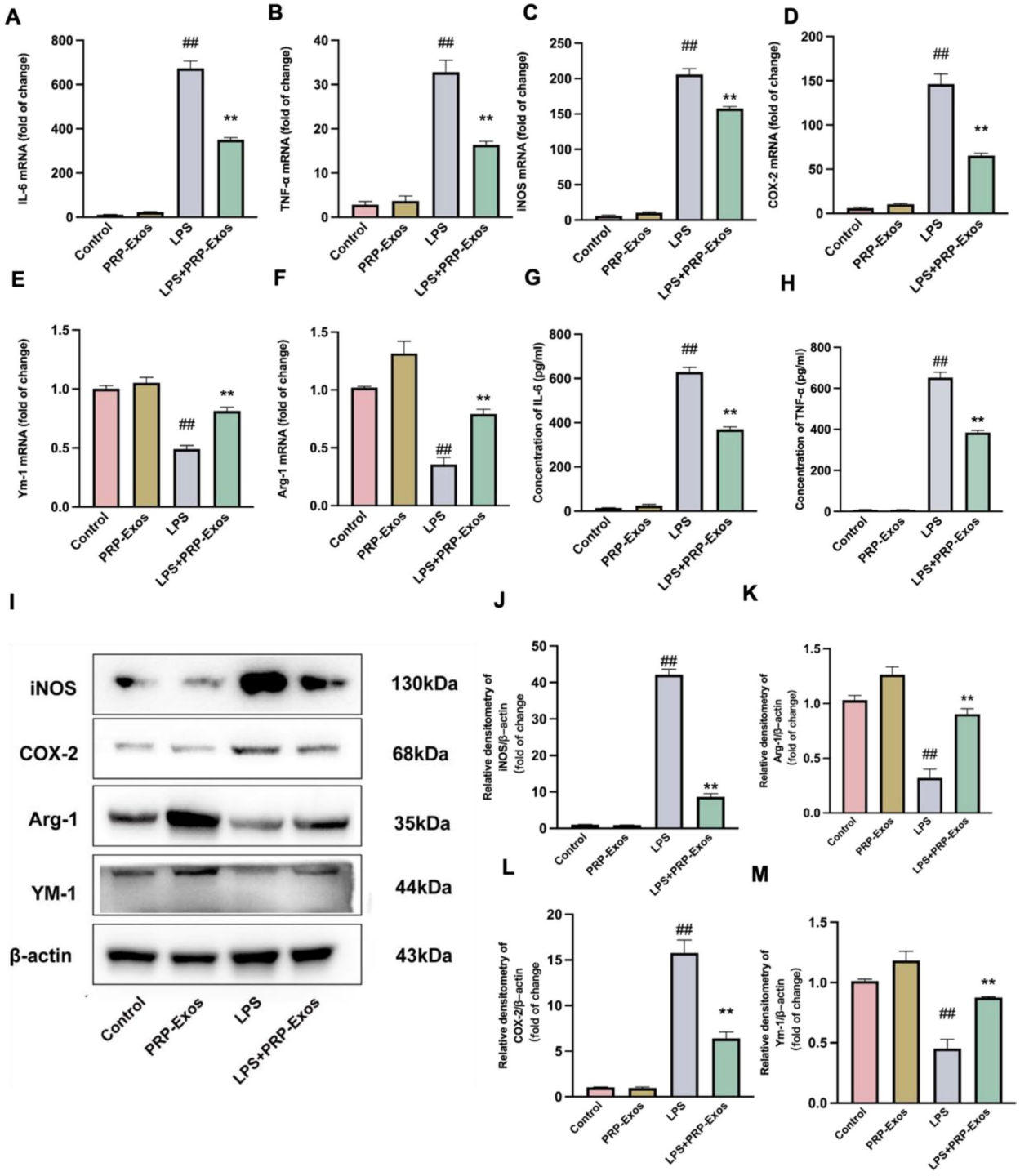

Fig. 2 PRP-Exos promote microglia M2 polarization and alleviate neuroinflammation in vitro. (**A**-**F**) The mRNA levels of M1 microglia markers (IL-6, TNF-α, iNOS, and COX-2) and M2 microglia markers (Ym-1, CD206, and Arg-1) were detected by RT-PCR. (**G**-**M**) The protein levels of M1 microglia markers and M2 microglia markers were measured using ELISA (IL-6 and TNF-α) and western blot (COX-2, iNOS, Arg-1, CD206, and Ym-1). Results are shown as means ± SEM ($n = 4$). # $p < 0.05$ and ## $p < 0.01$ vs. the control group; * $p < 0.5$ and ** $p < 0.01$ vs. the LPS-exposed group

using immunofluorescence techniques. Our results indicated that PRP-Exos markedly reduced the phosphorylation of NF-κB p65 (Fig. 3A, B) and IκB (Fig. 3A, C), inhibited the degradation of IκB (Fig. 3D) and nuclear migration of NF-κB p65 (Fig. 3E, F). These observations confirm that PRP-Exos effectively attenuate the activation of the NF-κB pathway in BV-2 cells exposed to LPS.

PRP-Exos enhance BSCB integrity in OGD-treated bEnd.3 cells

The integrity of the blood-spinal cord barrier (BSCB) is crucial for maintaining central nervous system homeostasis. This study assessed BSCB integrity by examining the expression of tight junction proteins ZO-1 and Claudin-3, which are fundamental to barrier function. In control groups subjected to oxygen-glucose deprivation (OGD), immunofluorescence staining showed a significant decrease in the fluorescence intensity of ZO-1 and Claudin-3, indicating impaired BSCB integrity. Conversely, treatment with PRP-Exos markedly increased the fluorescence intensity of these proteins (Fig. 4A, B, E, F), underscoring the potential of PRP-Exos to fortify BSCB structure.

Further analysis of the impact of PRP-Exos on bEnd.3 cell permeability utilized the bEnd.3 OGD model to monitor FITC-dextran transport pre- and post-OGD exposure (Fig. 4C). Initial findings revealed no significant difference in permeability among untreated groups

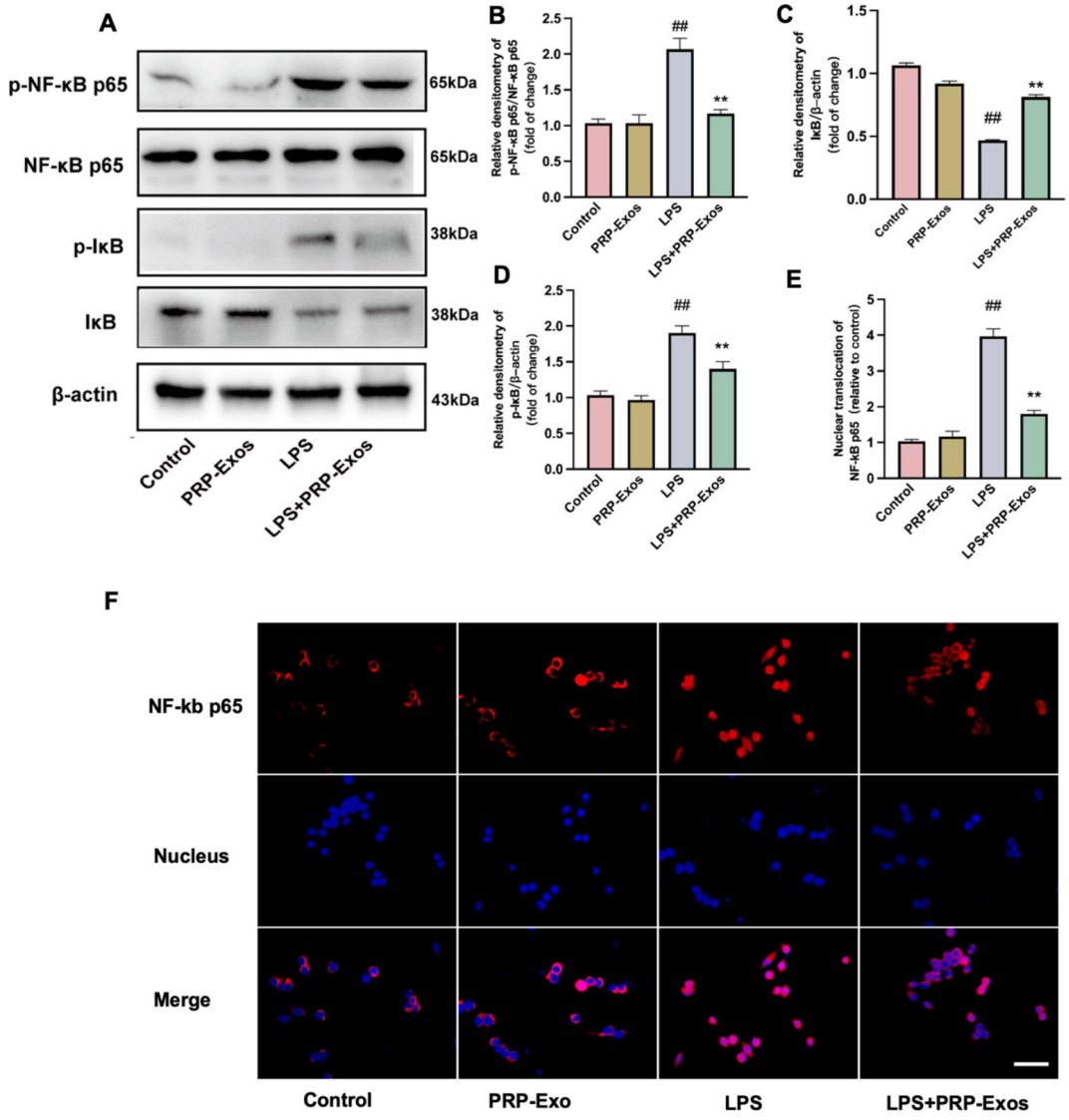

Fig. 3 PRP-Exos inhibit activation of NF-κB in LPS-exposed BV-2 cells. (**A**)The protein levels of IκB, NF-κB p65, and their phosphorylation were detected by western blot. (**B**) The levels of phos-NF-κB p65 were analyzed relative to NF-κB p65. (**C**, **D**) The levels of IκB and phos-IκB were analyzed relative to β-actin. (**E**, **F**) The nuclear translocation level of NF-κB p65 was examined by immunofluorescence staining (the scale bar represents 100 μm). # $p < 0.05$ and ## $p < 0.01$ vs. the control group; * $p < 0.5$ and ** $p < 0.01$ vs. the LPS-exposed group

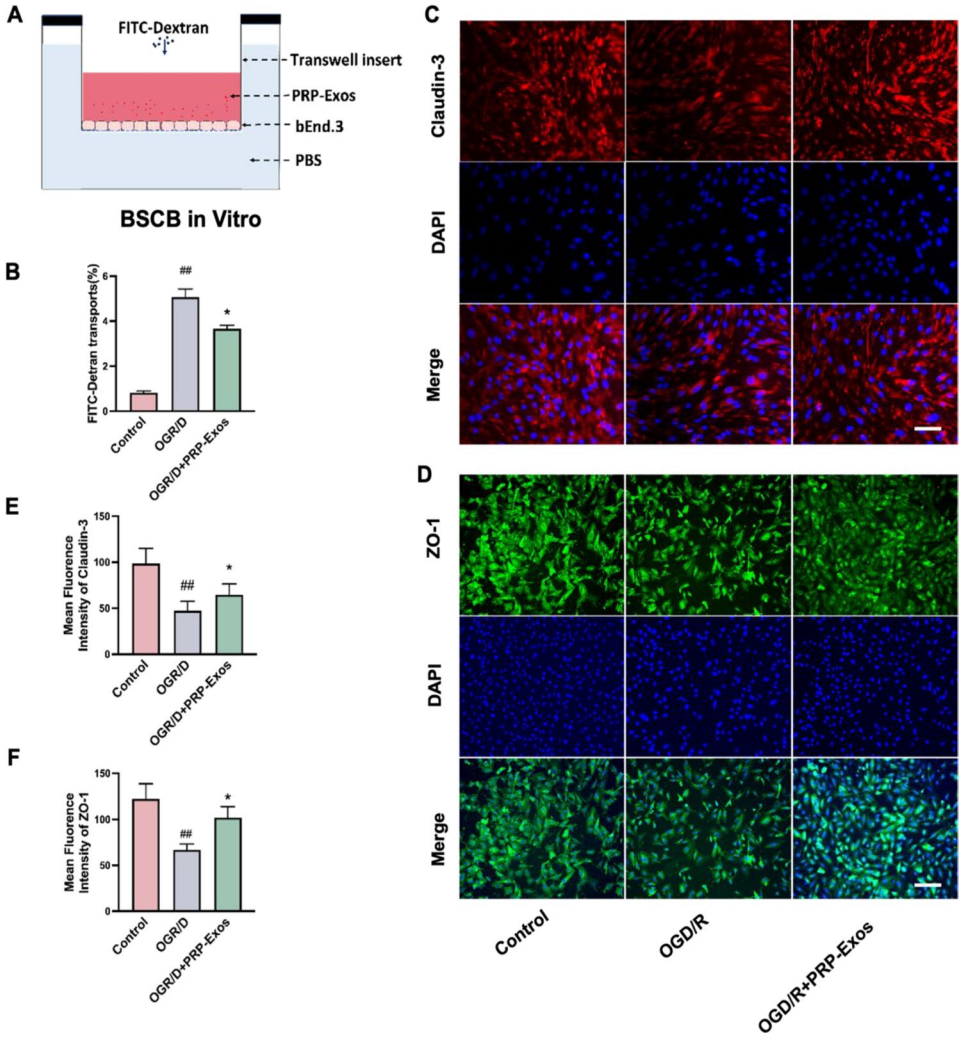

Fig. 4 PRP-Exos reduce the level of the permeability of the OGD-treated bEnd.3 in vitro. (**A**) Schematic diagram of the transwell FITC-dextran permeation assay; upper layer, bEnd.3 cells. (**B**) FITC-dextran transport assay of the permeability before and after OGD. $n=4$ per group. (**C**) Representative immunofluorescence images of tight junction-related protein (Claudin-3 and ZO-1). Scale bar, 100 μm. (**D**) Quantitative evaluation of the fluorescence intensity of Claudin-3 and ZO-1. # $p<0.05$ and ##$p<0.01$ vs. the control group; * $p<0.5$ and **$p<0.01$ vs. the OGD/R-exposed group

(Fig. 4D). However, a notable increase in FITC-dextran translocation post-OGD was significantly attenuated by PRP-Exos treatment. This reduction in permeability suggests that PRP-Exos may preserve tight junction integrity, a key element of paracellular barrier function, thereby enhancing BSCB integrity in the context of OGD stress.

PRP-Exos promote functional recovery after SCI

For local delivery, we used a hydrogel to deliver exosomes, and the PEG/ODEX Hydrogel demonstrated excellent slow release of exosomes (Figure S2). At 14 days post-surgery, we observed that PRP-Exos were still being released into the spinal cord in vitro and could be uptake by endothelial cells and microglia. We assessed motor function recovery post-spinal cord injury (SCI) in BMS scales. The data on weight and BMS scores (Fig. 5A, B) indicated limited hind limb recovery in the SCI and gel-treated groups. Administration of PRP-Exos notably improved motor function recovery after SCI. Additionally, PRP-Exos treatment increased mouse weight, suggesting an overall better condition of the mice. Mice in the PRP-Exos group largely regained normal physiological angles in their lower limbs, unlike those in the SCI and gel groups, which remained restricted (Fig. 5C).

Following 28 days of treatment, histopathological analysis of the injured spinal cord tissue was conducted using HE and Masson staining. The sham and SCI groups showed significant cavitation at the injury site (Fig. 5D, F). Conversely, PRP-Exos treatment substantially reduced cavity formation in the injured spinal cord region. Moreover, Masson's trichrome staining indicated that the PRP-Exos group had decreased collagen deposition and a more intact tissue structure.

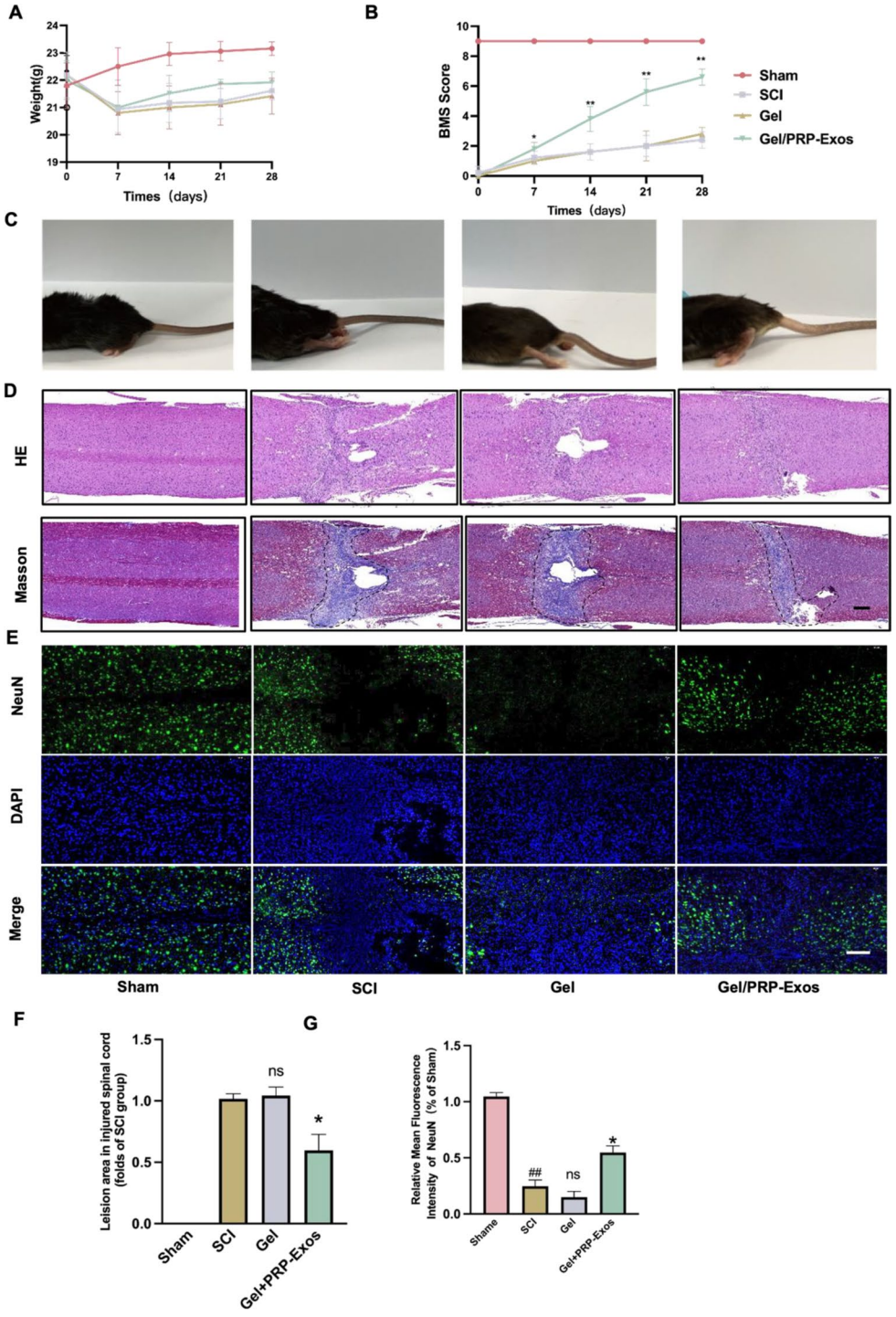

Fig. 5 The functional recovery of SCI mice after 4 weeks of PRP-Hydrogel treatment. (**A**, **B**) The Weight and BMS score of mice in each group ($n=4$). (**C**) The morphology of the hind limbs of the mice in each group during walking after 4 weeks. (**D**) Representative images of hematoxylin-eosin (HE) staining and Masson staining in each group. Scale bar: 200 μm. (**E**) Representative immunofluorescence images of NeuN (green), and DAPI (blue) in the SCI area. (**F**,**G**) Quantitative analysis of Leision area and NeuN relative mean fluorescence intensity in (**D**) and (**E**). Results are shown as means ± SEM ($n=4$).# $p<0.05$ and ## $p<0.01$ vs. the Sham group; *$p<0.05$ and**$p<0.01$ vs. the SCI group

Immunofluorescent staining was also performed to further validate the impact of PRP-Exos on neuronal recovery, with neurons marked by Green NeuN (Fig. 5E, G). Statistical analysis revealed no difference in fluorescence intensity between the SCI and hydrogel groups. However, a significant increase in fluorescence intensity was observed in the PRP-Exos/gel group compared to the prior groups.

These experimental results demonstrate that the combined strategy of PRP-Exos/gel can effectively promote the recovery of motor and neurological functions.

PRP-Exos modulate macrophage/microglia polarization towards M2 phenotype in vivo

PRP-Exos can promote the polarization of macrophages/microglia towards the M2 phenotype in vitro, but their influence on polarization direction in vivo was previously unclear. To investigate the potential M1 polarization of macrophages/microglia in vivo, immunofluorescence staining was conducted for the M1 phenotype marker iNOS. In the group treated with PRP-Exos, a significant reduction in iNOS-positive cells was observed (Fig. 6A, C). Conversely, to assess M2 polarization, immunofluorescence staining for the M2 phenotype marker Arg-1 was performed (Fig. 6B, D), showing a clear increase in the proportion of Arg-1-positive cells. These experimental results demonstrate that PRP-Exos can effectively promote the polarization of macrophages/microglia towards the M2 phenotype in vivo, indicating their therapeutic potential in modulating the inflammatory response.

PRP-Exos promote BSCB repair after SCI

To evaluate the efficacy of PRP-Exos in repairing the BSCB following SCI, we utilized Evans blue dye to assess BSCB permeability one day post-SCI across different treatment groups. PRP-Exos treatment significantly minimized Evans blue dye leakage at the injury site, indicating a reduction in BSCB permeability. This effect was visually apparent in spinal cord images, with gel treatment alone proving less effective compared to the combined PRP-Exo/Gel treatment (Fig. 7A). Following SCI, BSCB disruption facilitates neutrophil infiltration into the spinal cord and the subsequent release of matrix metalloproteinases (MMPs), culminating in the loss of tight junction proteins and further BSCB damage. Previous studies have documented a notable decline in the expression of tight junction proteins ZO-1 and occludin post-SCI. In our investigation, the PRP-Exos/Gel treatment significantly counteracted the decrease in ZO-1 and occludin-3 expression 28 days post-SCI (Fig. 7B-C). These results underscore the potent capability of PRP-Exos/Gel to repair the BSCB.

The role of PRP-Exos in enhancing spinal cord repair after SCI

Further analysis aimed to determine the extent of spinal cord injury, neuronal survival, and glial scar formation, employing immunofluorescence staining for Glial Fibrillary Acidic Protein (GFAP) in red and NEURON-SPECIFIC CLASS III BETA-TUBULIN (Tuj-1), across various groups on day 28 post-SCI. Our findings indicated that PRP-Exos treatment led to a significant reduction in lesion volume and an increase in the relative mean intensity of Tuj-1 in the PRP-Exos group compared to the SCI control group (Fig. 8A). Additionally, the PRP-Exos/Gel group exhibited lower levels of GFAP, indicative of reduced glial scarring. These observations suggest that PRP-Exos/Gel treatment mitigates spinal cord damage and enhances neuronal health, highlighting its therapeutic potential in spinal cord repair post-SCI.

Discussion

Spinal cord injury represents a severe medical condition characterized by profound motor, sensory, and autonomic dysfunctions, significantly affecting individuals' quality of life and imposing a substantial economic burden [1, 25–27]. The initial mechanical insult to the BSCB following SCI triggers a cascade of secondary inflammatory, vasolytic, and biochemical responses that exacerbate neuronal dysfunction [28, 29]. Currently, the management of acute SCI primarily involves surgical intervention and administration of high-dose methylprednisolone, the efficacy of which is still debated [1, 26, 27]. The destruction of the BSCB facilitates the continuous infiltration of inflammatory cells into the spinal cord, perpetuating inflammation phases ranging from acute to chronic stages, thereby limiting the effectiveness of anti-inflammatory agents. A therapeutic agent capable of both repairing the BSCB and modulating inflammation could significantly mitigate inflammatory damage, reduce neuronal apoptosis, and foster early neurological recovery post-SCI [2, 23, 29]. Exosomes, including those derived from PRP-Exos, have been identified as potential agents for neuronal repair, inflammation modulation, and BSCB restoration, yet their specific roles in angiogenesis, inflammation, and tissue regeneration post-SCI have only begun to be explored [30–33].

Our study successfully isolated and characterized PRP-Exos(Fig. 1), highlighting their potential as an accessible bioactive substance that can promote functional recovery after SCI by modulating neuroinflammation and attenuating BSCB injury .

The dynamic polarization of macrophages/microglia in response to the SCI microenvironment plays a pivotal role in regulating the immune microenvironment and facilitating tissue repair. While M1 macrophages contribute to inflammation and hinder axonal regeneration, M2

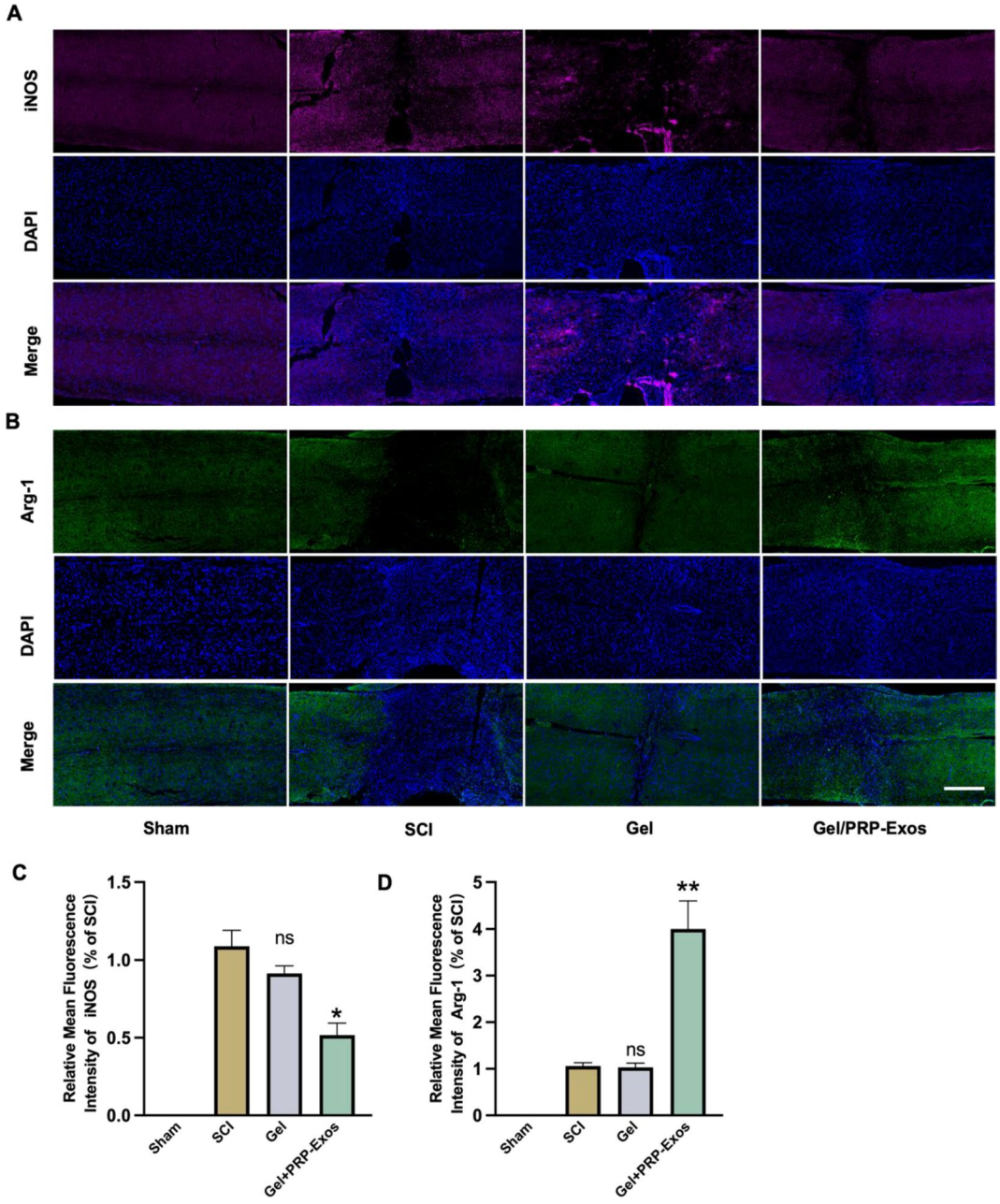

Fig. 6 Effects of PRP-Exos on NSC Differentiation Post-SCI (**A**)Representative immunofluorescence images of iNOS(Red), and DAPI (blue) in the SCI area. Scale bar 200 μm. (**C**) Representative immunofluorescence images of Arg-1(green), and DAPI (blue) in the SCI area. Scale bar 200 μm. (**D**, **E**) Quantitative analysis of iNOS and Arg-1 relative mean fluorescence intensity in (**A**) and (**B**). Results are shown as means ± SEM ($n = 4$).# $p < 0.05$ and ## $p < 0.01$ vs. the Sham group; *$p < 0.05$ and**$p < 0.01$ vs. the SCI group

macrophages promote wound healing and tissue remodeling through the release of anti-inflammatory cytokines [34–36]. Our study illustrates the capacity of PRP-Exos to stimulate M2 polarization in vitro by modulating the NF-κB signaling pathway, highlighting their potential in SCI treatment strategies focused on inflammation modulation. (Figures 2 and 3)

Furthermore, the integrity of the BSCB is crucial for spinal cord function. Disruption of the BSCB, a common aftermath of SCI, results in vascular damage at the injury site and permanent alterations distal to the injury [2]. Our findings indicate that PRP-Exos exert protective effects on the BSCB in vivo and in vitro, enhancing neurological function recovery post-SCI.The regulation of tight junction proteins, such as claudin-3 and ZO-1, is essential for BSCB permeability post-SCI(Figs. 4 and 7). Our data corroborate the reduction of these proteins following SCI, underscoring the disruption of cellular junctions as a

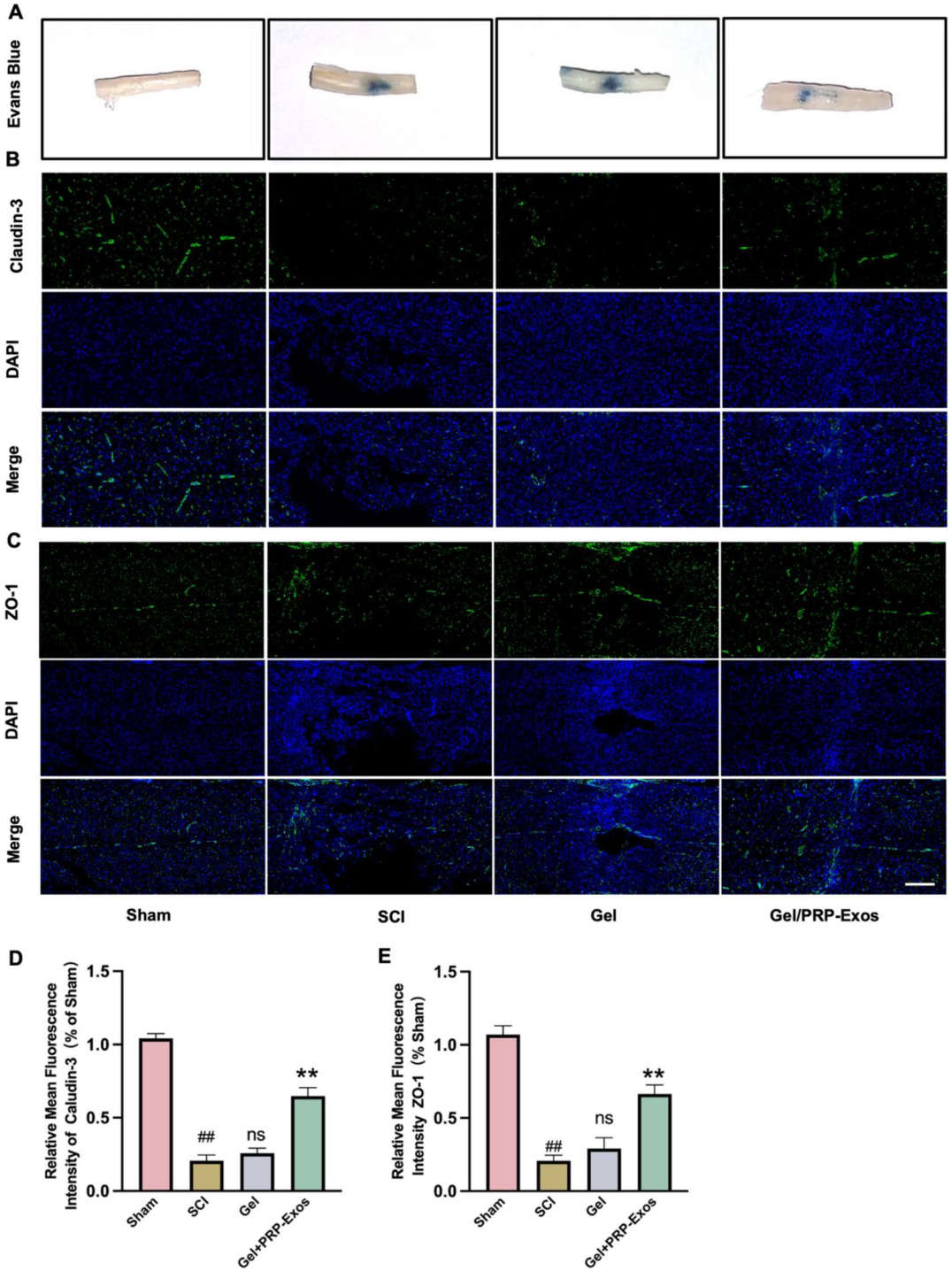

Fig. 7 PRP-Exos stabilize BSCB in vivo. (**A**) Representative digital pictures of spinal cord samples from EB leakage tests. (**B**-**C**) Representative immunofluorescence images of Claudin-3 (green), and DAPI (blue) in the SCI area. Scale bar 100 μm. (**C**) Representative immunofluorescence images of ZO-1(green), and DAPI (blue) in the SCI area. Scale bar 200 μm. (**D**, **E**) Quantitative analysis of Claudin-3 and ZO-1 relative mean fluorescence intensity in (**B**) and (**C**). Results are shown as means ± SEM ($n = 4$). # $p < 0.05$ and ## $p < 0.01$ vs. the Sham group; *$p < 0.05$ and**$p < 0.01$ vs. the SCI group

primary factor in BSCB damage. This disruption allows for immune cell infiltration, further aggravating secondary SCI damage. Previous studies have shown that certain interventions can mitigate BSCB disruption by inhibiting matrix metalloproteinases (MMPs) and preserving tight junction structures [23]. Our research adds to this body of evidence, demonstrating that PRP-Exos reduce tissue permeability, reduce exudation at the injury site, and

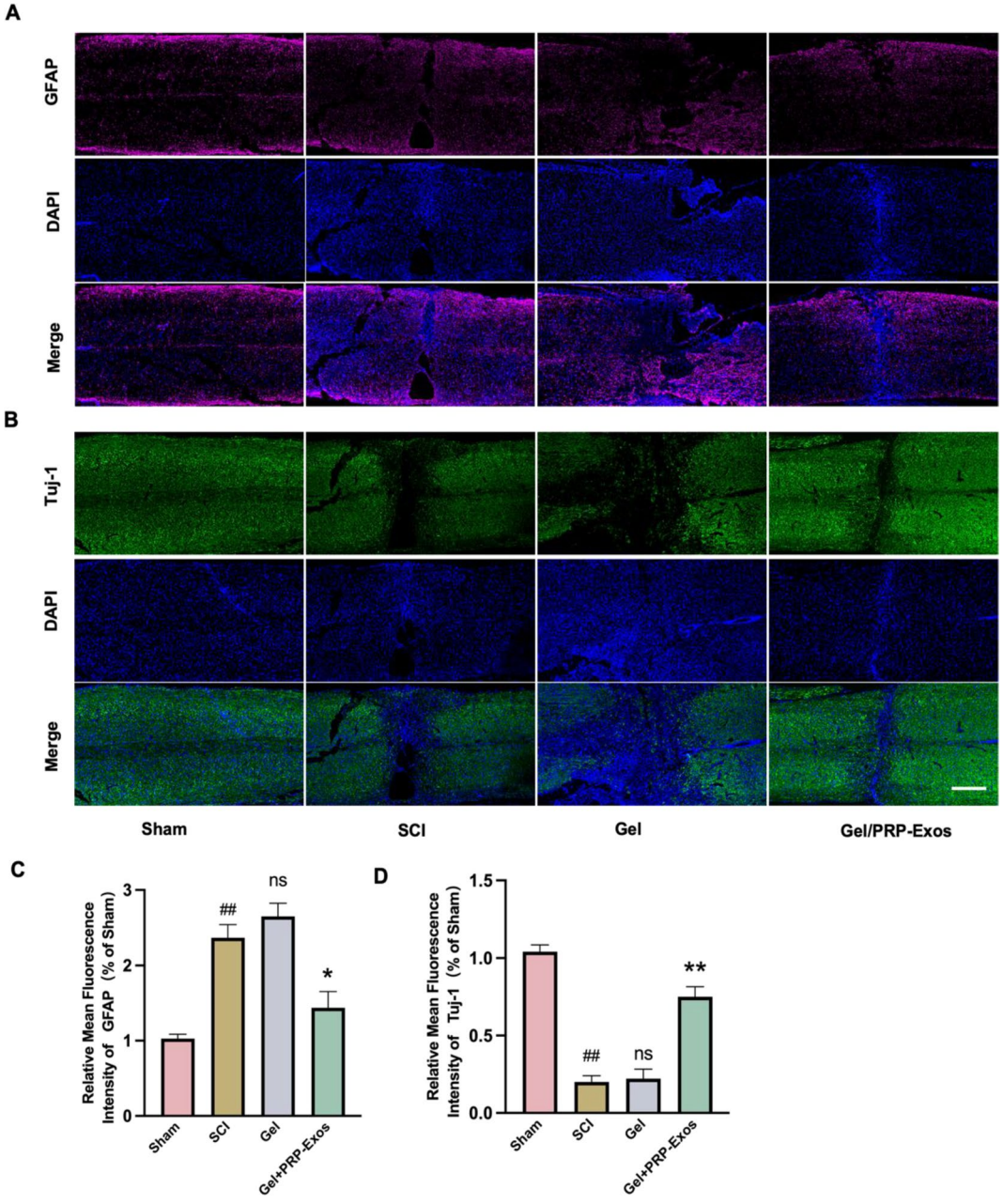

Fig. 8 Effects of PRP-Exos on NSC Differentiation Post-SCI (**A**) Representative immunofluorescence images of GFAP(Red), and DAPI (blue) in the SCI area. Scale bar 200 μm. (**C**) Representative immunofluorescence images of Tuj-1(green), and DAPI (blue) in the SCI area. Scale bar 200 μm. (**D**, **E**) Quantitative analysis of GFAP and Tuj-1 relative mean fluorescence intensity in (**A**) and (**B**). Results are shown as means ± SEM ($n = 4$).## $p < 0.01$vs. the Sham group; **$p < 0.01$vs. the SCI group

increase the expression of tight junction proteins, thereby affirming their significant reparative effect on intercellular junctions after SCI(Fig. 9).

However, our study has limitations, primarily focusing on the anti-inflammatory effects of PRP-Exos without delving into neuroproliferation, differentiation, and axonal regeneration. Additionally, while confirming M2 polarization induction by PRP-Exos, we did not investigate the specific components responsible for this effect, which warrants further research. Our in vivo experiments showcased PRP-Exos' ability to mitigate localized inflammatory responses and potentially attenuate systemic inflammation, underpinning the importance of local immunomodulation in creating a conducive environment for neuronal repair.

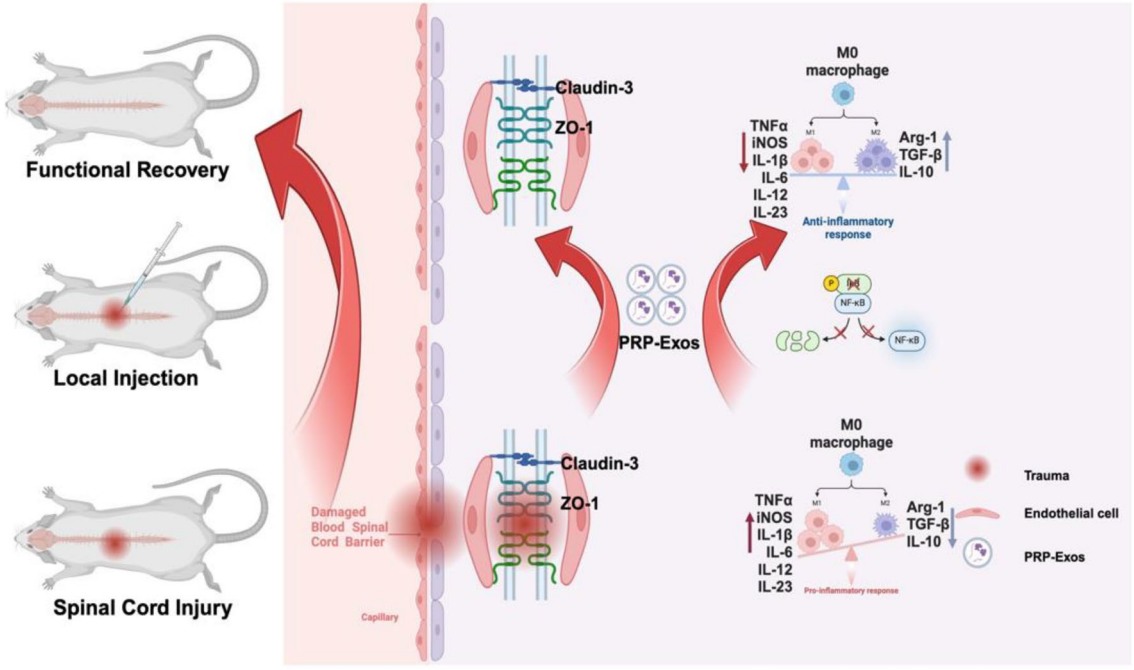

Fig. 9 Schematic of platelet-rich plasma- derived exosomes promote blood-spinal cord barrier repair and attenuate neuroinflammation after spinal cord injury

Conclusion

This discussion integrates our study's results, emphasizing PRP-Exos' role in promoting BSCB repair and neuroinflammatory modulation post-SCI. The promising outcomes suggest a novel avenue for SCI treatment, focusing on exosome-mediated pathways for enhancing neurological recovery and functional restoration. Future investigations should aim to unravel the specific molecular mechanisms of PRP-Exos and expand our understanding of their therapeutic potential in SCI and other neurodegenerative conditions.

Supplementary Information

The online version contains supplementary material available at https://doi.org/10.1186/s12951-024-02737-5.

Supplementary Material 1

Acknowledgements
Figures were created in https://Biorender.com.

Author contributions
Conceptualization: Xinyu Nie, Yanting Liu, Qinyi Liu; Methodology: Xinyu Nie, Tianyang Yu, Tong Yu; Investigation: Yanting Liu, Zhihe Yun, Wu Xue; Writing-original draft: Xinyu Nie, Yanting Liu, Tao Yu, Junyan An, Anyuan Dai, Kun Wu, Qinyi Liu.

Funding
This study was supported by Graduate Innovation Fund of Jilin University, Jilin Provincial Department of Education Science and Technology Research Project (JJKH20211157KJ), Jilin Provincial Natural Science Foundation (20210101265JC), Jilin Provincial Science and Technology Department Project(No.YDZJ202301ZYTS032).

Data availability
No datasets were generated or analysed during the current study.

Declarations

Ethics approval and consent to participate
All procedures approval from the Animal Care and Use Committee at Jilin University(SY202104011).

Consent for publication
Not applicable.

Competing interests
The authors declare no competing interests.

Received: 26 March 2024 / Accepted: 23 July 2024
Published online: 31 July 2024

References

1. Izzy S. Traumatic spinal cord Injury. Continuum (Minneapolis Minn). 2024;30:53–72.
2. Jin L, Li J, Wang K, Xia W, Zhu Z, Wang C, et al. Blood-spinal cord barrier in spinal cord Injury: a review. J Neurotraum. 2021;38:1203–24.
3. Tran A, Warren P, Silver J. The Biology of Regeneration failure and success after spinal cord Injury. Physiol Rev. 2018;98:881–917.
4. Hu X, Xu W, Ren Y, Wang Z, He X, Huang R, et al. Spinal cord injury: molecular mechanisms and therapeutic interventions. Signal Transduct Tar. 2023;8:245.
5. Ribeiro B, daCruz B, deSousa B, Correia P, David N, Rocha C, et al. Cell therapies for spinal cord injury: a review of the clinical trials and cell-type therapeutic potential. Brain. 2023;146:2672–93.
6. Saumell-Esnaola M, Delgado D, GarciaDelCano G, Beitia M, Salles J, Gonzalez-Burguera I et al. Isolation of platelet-derived exosomes from human platelet-rich plasma: biochemical and morphological characterization. Int J Mol Sci. 2022;23.
7. Bohren Y, Timbolschi D, Muller A, Barrot M, Yalcin I, Salvat E. Platelet-rich plasma and cytokines in neuropathic pain: a narrative review and a clinical perspective. Eur J Pain. 2022;26:43–60.

8. Zhang Y, Wang X, Chen J, Qian D, Gao P, Qin T, et al. Exosomes derived from platelet-rich plasma administration in site mediate cartilage protection in subtalar osteoarthritis. J Nanobiotechnol. 2022;20:56.
9. Everts P, Knape J, Weibrich G, Schonberger J, Hoffmann J, Overdevest E, et al. Platelet-rich plasma and platelet gel: a review. J Extracorpor Technol. 2006;38:87–174.
10. Kalluri R, LeBleu VS. The biology, function, and biomedical applications of exosomes. Volume 367. New York, N.Y: Science; 2020.
11. Doyle LM, Wang MZ. Overview of Extracellular vesicles, their origin, composition, purpose, and methods for Exosome isolation and analysis. Cells-Basel. 2019;8.
12. He C, Zheng S, Luo Y, Wang B. Exosome Theranostics: Biology and Translational Medicine. Theranostics. 2018;8:237–55.
13. Nie X, Yuan T, Yu T, Yun Z, Yu T, Liu Q. Non-stem cell-derived exosomes: a novel therapeutics for neurotrauma. J Nanobiotechnol. 2024;22:108.
14. Han M, Yang H, Lu X, Li Y, Liu Z, Li F, et al. Three-dimensional-cultured MSC-Derived exosome-hydrogel hybrid microneedle array Patch for spinal cord repair. Nano Lett. 2022;22:6391–401.
15. Yu T, Yang L, Zhou Y, Wu M, Jiao J. Exosome-mediated repair of spinal cord injury: a promising therapeutic strategy. Stem Cell Res Ther. 2024;15:6.
16. Qian J, Wang X, Su G, Shu X, Huang Z, Jiang H, et al. Platelet-rich plasma-derived exosomes attenuate intervertebral disc degeneration by promoting NLRP3 autophagic degradation in macrophages. Int Immunopharmacol. 2022;110:108962.
17. Liu X, Wang L, Ma C, Wang G, Zhang Y, Sun S. Exosomes derived from platelet-rich plasma present a novel potential in alleviating knee osteoarthritis by promoting proliferation and inhibiting apoptosis of chondrocyte via Wnt/beta-catenin signaling pathway. J Orthop Surg Res. 2019;14:470.
18. Tao S, Yuan T, Rui B, Zhu Z, Guo S, Zhang C. Exosomes derived from human platelet-rich plasma prevent apoptosis induced by glucocorticoid-associated endoplasmic reticulum stress in rat osteonecrosis of the femoral head via the Akt/Bad/Bcl-2 signal pathway. Theranostics. 2017;7:733–50.
19. Guo S, Tao S, Yin W, Qi X, Yuan T, Zhang C. Exosomes derived from platelet-rich plasma promote the re-epithelization of chronic cutaneous wounds via activation of YAP in a diabetic rat model. Theranostics. 2017;7:81–96.
20. Akbari-Gharalari N, Ghahremani-Nasab M, Naderi R, Aliyari-Serej Z, Karimi-pour M, Shahabi P, et al. Improvement of spinal cord injury symptoms by targeting the Bax/Bcl2 pathway and modulating TNF-alpha/IL-10 using platelet-rich plasma exosomes loaded with dexamethasone. Aims Neurosci. 2023;10:332–53.
21. Wu J, Piao Y, Liu Q, Yang X. Platelet-rich plasma-derived extracellular vesicles: a superior alternative in regenerative medicine? Cell Proliferat. 2021;54:e13123.
22. Rui S, Yuan Y, Du C, Song P, Chen Y, Wang H, et al. Comparison and investigation of Exosomes derived from platelet-rich plasma activated by different agonists. Cell Transpl. 2021;30:9636897211017833.
23. Xie Y, Sun Y, Liu Y, Zhao J, Liu Q, Xu J, et al. Targeted delivery of RGD-CD146(+) CD271(+) human umbilical cord mesenchymal stem cell-derived Exosomes promotes blood-spinal cord barrier repair after spinal cord Injury. ACS Nano. 2023;17:18008–24.
24. ZhipingQi, TianhuiZhang. WeijianKong. A dual-drug enhanced injectable hydrogel incorporated with neural stem cells for combination therapy in spinal cord injury. Chem Eng J. 2022;427.
25. Albashari A, He Y, Luo Y, Duan X, Ali J, Li M et al. Local spinal cord Injury Treatment using a Dental Pulp Stem Cell Encapsulated H(2) S releasing multifunctional Injectable Hydrogel. Adv Healthc Mater. 2023e2302286.
26. Karsy M, Hawryluk G. Modern Medical Management of spinal cord Injury. Curr Neurol Neurosci. 2019;19:65.
27. Hornby TG, Reisman DS, Ward IG, Scheets PL, Miller A, Haddad D, et al. Clinical Practice Guideline to improve locomotor function following chronic stroke, incomplete spinal cord Injury, and Brain Injury. J Neurologic Phys Therapy: JNPT. 2020;44:49–100.
28. Al Mamun A, Wu Y, Monalisa I, Jia C, Zhou K, Munir F, et al. Role of pyroptosis in spinal cord injury and its therapeutic implications. J Adv Res. 2021;28:97–109.
29. Tran AP, Warren PM, Silver J. The Biology of Regeneration failure and success after spinal cord Injury. Physiol Rev. 2018;98:881–917.
30. Zhang C, Li D, Hu H, Wang Z, An J, Gao Z, et al. Engineered extracellular vesicles derived from primary M2 macrophages with anti-inflammatory and neuroprotective properties for the treatment of spinal cord injury. J Nanobiotechnol. 2021;19:373.
31. Gao Z, Zhang C, Xia N, Tian H, Li D, Lin J, et al. Berberine-loaded M2 macrophage-derived exosomes for spinal cord injury therapy. Acta Biomater. 2021;126:211–23.
32. Yuan X, Wu Q, Wang P, Jing Y, Yao H, Tang Y, et al. Exosomes Derived from Pericytes Improve Microcirculation and protect blood-spinal cord barrier after spinal cord Injury in mice. Front Neurosci-Switz. 2019;13:319.
33. Ge X, Zhou Z, Yang S, Ye W, Wang Z, Wang J, et al. Exosomal USP13 derived from microvascular endothelial cells regulates immune microenvironment and improves functional recovery after spinal cord injury by stabilizing IkappaBalpha. Cell Bioscience. 2023;13:55.
34. Bourgeois-Tardif S, De Beaumont L, Rivera JC, Chemtob S, Weil AG. Role of innate inflammation in traumatic brain injury. Neurol Sciences: Official J Italian Neurol Soc Italian Soc Clin Neurophysiol. 2021;42:1287–99.
35. Freyermuth-Trujillo X, Segura-Uribe JJ, Salgado-Ceballos H, Orozco-Barrios CE, Coyoy-Salgado A. Inflammation: a target for treatment in spinal cord Injury. Cells-Basel. 2022;11.
36. Li Y, Ritzel RM, Khan N, Cao T, He J, Lei Z, et al. Delayed microglial depletion after spinal cord injury reduces chronic inflammation and neurodegeneration in the brain and improves neurological recovery in male mice. Theranostics. 2020;10:11376–403.

Publisher's Note